

---

Final Report to AFOSR / AOARD

# High Temperature Deformation Behavior of HCP Alloys

- An Internal Variable Approach

Professor Young Won Chang  
Center for Advanced Aerospace Materials  
Department of Materials Science and Engineering  
Pohang University of Science and Technology

May 31, 2006

## Abstract

The high temperature deformation behavior of HCP alloys has been investigated within the framework of an internal variable theory. Various mechanical tests were conducted to this end for AZ31 Mg and Ti-6Al-4V alloys together with microstructure observation. In the first part, a series of load relaxation tests was first performed for AZ31 Mg alloy to obtain overall flow curves, which were then analyzed according to the respective physical mechanisms, viz., the grain boundary sliding (GBS) and the accommodating dislocation glide process as prescribed by the internal variable theory proposed by the authors. Many valuable data were obtained in this

Report Documentation Page		Form Approved OMB No. 0704-0188
Public reporting burden for the collection of information is estimated to average 1 hour per response, including the time for reviewing instructions, searching existing data sources, gathering and maintaining the data needed, and completing and reviewing the collection of information. Send comments regarding this burden estimate or any other aspect of this collection of information, including suggestions for reducing this burden, to Washington Headquarters Services, Directorate for Information Operations and Reports, 1215 Jefferson Davis Highway, Suite 1204, Arlington VA 22202-4302. Respondents should be aware that notwithstanding any other provision of law, no person shall be subject to a penalty for failing to comply with a collection of information if it does not display a currently valid OMB control number.		
1. REPORT DATE <b>27 JUL 2006</b>	2. REPORT TYPE <b>Final Report (Technical)</b>	3. DATES COVERED <b>25-04-2005 to 21-07-2006</b>
4. TITLE AND SUBTITLE <b>High-temperature deformation behavior of HCP alloys - an internal variable approach</b>		5a. CONTRACT NUMBER <b>FA520905P0390</b>
		5b. GRANT NUMBER
		5c. PROGRAM ELEMENT NUMBER
6. AUTHOR(S) <b>Young Won Chang</b>		5d. PROJECT NUMBER
		5e. TASK NUMBER
		5f. WORK UNIT NUMBER
7. PERFORMING ORGANIZATION NAME(S) AND ADDRESS(ES) <b>Pohang University of Science and Technology, San 31, Hyoja-dong, Nam-gu, Pohang 790-784, Korea (South), KE, 790-784</b>		8. PERFORMING ORGANIZATION REPORT NUMBER <b>AOARD-054032</b>
9. SPONSORING/MONITORING AGENCY NAME(S) AND ADDRESS(ES) <b>The US Resarch Labolatory, AOARD/AFOSR, Unit 45002, APO, AP, 96337-5002</b>		10. SPONSOR/MONITOR'S ACRONYM(S) <b>AOARD/AFOSR</b>
		11. SPONSOR/MONITOR'S REPORT NUMBER(S) <b>AOARD-054032</b>
12. DISTRIBUTION/AVAILABILITY STATEMENT <b>Approved for public release; distribution unlimited</b>		
13. SUPPLEMENTARY NOTES		
14. ABSTRACT <p><b>The high temperature deformation behavior of HCP alloys has been investigated within the framework of an internal variable theory. Various mechanical tests were conducted to this end for AZ31 Mg and Ti-6Al-4V alloys together with microstructure observation. In the first part, a series of load relaxation tests was first performed for AZ31 Mg alloy to obtain overall flow curves, which were then analyzed according to the respective physical mechanisms, viz., the grain boundary sliding (GBS) and the accommodating dislocation glide process as prescribed by the internal variable theory proposed by the authors. Many valuable data were obtained in this way, providing new physical insight as well as a more comprehensive understanding about the superplastic deformation behavior of AZ31Mg alloy. In the second part of this work, load relaxation and creep tests for hot rolled Ti-6Al-4V alloy have also been conducted to clarify specifically the effect of textures on the deformation behavior of this Ti alloy below 700 °C and the results were then again analyzed according to the internal variable approach. The values of internal strength variable <math>\sigma^*</math> were found to vary significantly by the textures, but not by the test temperature, while the texture effect was found to decrease at higher temperatures. The effect of texture was also observed to decrease by raising test temperature or by reducing the applied stress in creep tests, suggesting that glide assisted dislocation climb was activated at higher temperature and lower stress.</b></p>		
15. SUBJECT TERMS <b>Metals and Alloys, Materials Processing, Metabolic Engineering</b>		

16. SECURITY CLASSIFICATION OF:			17. LIMITATION OF ABSTRACT	18. NUMBER OF PAGES <b>26</b>	19a. NAME OF RESPONSIBLE PERSON
a. REPORT <b>unclassified</b>	b. ABSTRACT <b>unclassified</b>	c. THIS PAGE <b>unclassified</b>			

---

way, providing new physical insight as well as a more comprehensive understanding about the superplastic deformation behavior of AZ31Mg alloy.

In the second part of this work, load relaxation and creep tests for hot rolled Ti-6Al-4V alloy have also been conducted to clarify specifically the effect of textures on the deformation behavior of this Ti alloy below 700 °C and the results were then again analyzed according to the internal variable approach. The values of internal strength variable  $\sigma^*$  were found to vary significantly by the textures, but not by the test temperature, while the texture effect was found to decrease at higher temperatures. The effect of texture was also observed to decrease by raising test temperature or by reducing the applied stress in creep tests, suggesting that glide assisted dislocation climb was activated at higher temperature and lower stress.

## **Contents**

1. Introduction
2. Internal variables theory
3. AZ31 Mg alloy
  - Experimental procedures
  - Results and discussions
  - Summary
4. Ti-6V-4Al Alloy
  - Experimental procedures
  - Results and discussions
  - Summary
5. References

---

## 6. Publications and presentations

### 1. Introduction

Magnesium alloys hold the limelight as structural materials due to their excellent properties such as lightweight, high specific strength, and superior damping capacity. The use of magnesium alloy has significantly increased recently especially in the automotive industry. Magnesium alloys are generally fabricated by die casting process in view of high productivity, suitable strength, quality, and dimensional control. On the other hand, wrought magnesium alloys have superior ductility and strength than the die casting. They exhibit, however, low ductility near room temperature due to the limited slip systems inherent in HCP crystals. Magnesium alloys, therefore, need to be deformed at higher temperatures in order to obtain adequate ductility required for plastic forming. There have been numerous efforts to develop an optimum plastic forming process to enlarge the structural use of magnesium alloys [1-3]. For example, Watanabe and his coworkers reported extensively about the superplastic deformation behavior of various magnesium alloys, such as powder metallurgy processed ZK61, ECAE produced ZK60, warm-rolled AZ31, extruded AZ61, and so on [4-7]. In spite of numerous previous studies, it is believed that the high temperature deformation behavior of magnesium alloys including superplastic characteristics has not been adequately understood so far.

In case of Ti-6Al-4V alloy as a HCP alloy, deformation behavior is well known to depend on microstructures as well as textures developed during the prior deformation processes. The  $\alpha$  phase texture is generally known to strongly affect the deformation behavior up to about 600 °C due to limited available slip systems below this temperature. Sheet products manufactured by hot rolling process exhibit a strong deformation texture depending significantly on the rolling

temperature, microstructure, and phase volume fraction of constituent phases. It is therefore necessary to analyze the formation and evolution of texture from the various initial microstructures during hot rolling process to quantify the relation between texture and deformation properties.

High temperature deformation behavior of HCP alloys have long been described by a power law relationship between the two external variables, viz. flow stress ( $\sigma$ ) and strain rate ( $\dot{\epsilon}$ ), with the strain rate sensitivity parameter  $m$  as its power index [8, 9]. This phenomenological relationship is believed in this study not suitable to describe adequately high temperature deformation behavior of HCP alloys. It is therefore attempted to characterize the deformation behavior of HCP alloys, such as AZ31 Mg and Ti-6Al-4V alloy, by utilizing an internal variable theory proposed by Chang [10]. The theory has been applied successfully to characterize the high temperature deformation behavior of various metallic materials such as Al alloys, Pb-Sn hyper-eutectic alloy, and duplex stainless steels as reported in the previous studies [11-15]. In the following section, this internal variable theory will briefly be introduced first in the light of present work.

## **2. Internal variables theory**

### **Inelastic deformation.**

The theory prescribes inelastic deformation (GMD) to be the simultaneous processes of an accumulation of internal strain and a relaxation through a plastic strain within the framework of dislocation dynamics as schematically represented in Fig. 1. By further considering dislocation kinetics for this model, the following kinematics and stress relation among the deformation state variables could be derived,

$$\begin{aligned} \dot{\epsilon} &= \dot{\alpha} + \dot{\alpha}(1) \\ \mathbf{s} &= \mathbf{s}^I + \mathbf{s}^F \end{aligned} \quad (2)$$

with  $\dot{\alpha}$  denoting the co-rotational material time derivative of an internal strain similar to that prescribed by Hart [16] and  $\dot{\alpha}$  the rate of plastic strain. The stress variables  $\mathbf{s}^I$  and  $\mathbf{s}^F$  represent

the internal stress to overcome a long range interaction force among gliding dislocations and the friction stress due to a short range interaction between a glide dislocation and the lattice, respectively.

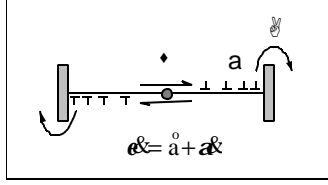


Fig. 1 Dislocations pile up against strong barriers during inelastic deformation.

Plastic strain rate and internal strain rate can be regarded as a mechanical activation process by internal stress and a viscous flow under a frictional drag of lattice, respectively. From these analogies, the following scalar relation can also be prescribed,

$$(\dot{\epsilon}^*/\dot{\epsilon}^I) = \exp(\sigma^*/\alpha^I)^p \quad (3)$$

$$(\dot{\epsilon}/\dot{\epsilon}_0) = (\sigma^F/\Sigma_0 - 1)^{\frac{1}{M}} \quad (4)$$

with  $p$  and  $M$  denoting material constants. The parameters  $\sigma^*$  and  $\Sigma_0$  represent the internal strength and critical static friction stress with  $\alpha^*$  and  $\epsilon_0$  their conjugate reference strain rate, respectively.

#### **Grain boundary sliding (GBS)**

In case of superplastic deformation, additional strain rate component due to GBS should be introduced as illustrated in Fig. 2(a) to give

$$\dot{\epsilon}_T = \dot{\epsilon}_0 + \dot{\epsilon}_d + \dot{\epsilon}_g \quad (5)$$

with  $g$  denoting the strain rate due to GBS. Since GBS can be regarded as a stress-induced viscous flow under a frictional drag, the following state equation similar to that given by Eq. (4) can be prescribed for the GBS,

$$\left(\frac{\dot{\gamma}}{\dot{\gamma}_0}\right) = \left(\frac{\sigma}{\Sigma_g} - 1\right)^{M_g} \quad (6)$$

with  $M_g$  denoting a characteristic exponent. The parameters  $\Sigma_g$  and  $\dot{\gamma}_0$  represent the critical static friction strength and its conjugate reference GBS strain rate, respectively. A rheological model given in Fig. 2(b) shows the kinematics correlation of these state variables. The details of theoretical development and definitions of constitutive parameters can be found in the references [10, 14].

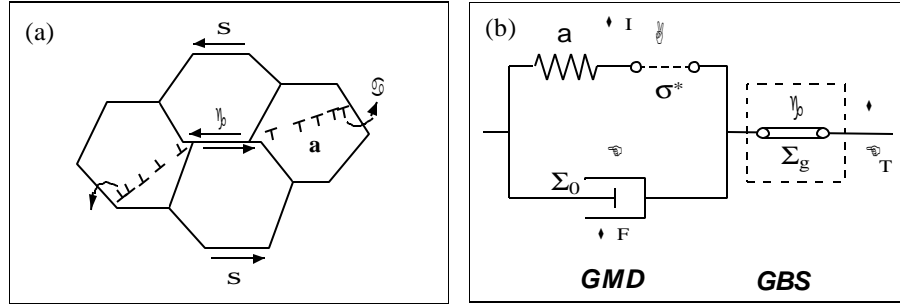


Fig. 2 An internal variable model for SSP: (a) topological and (b) rheological view.

### Dislocation climb.

Thermally activated dislocation climb can induce time dependent creep deformation in high temperature range. Since it can be considered as a process parallel to plastic straining (a) with similar kinetics of mechanical activation, dislocation creep rate (b) can also be introduced to the predefined kinematics and stress relation to give,

$$\dot{\epsilon} = \frac{\dot{\epsilon}_0}{a} + \dot{\epsilon}_a + \dot{\epsilon}_b \quad (7)$$

$$\left(\frac{\dot{\epsilon}_b}{\dot{\epsilon}_a}\right) = \exp\left(\frac{\dot{\epsilon}_b^*}{\dot{\epsilon}_a^*}\right)^{p_b} \quad (8)$$

where  $p_b$  is a characteristic exponent of creep activation similar to  $p_a$ . The parameters  $\dot{\epsilon}_b^*$  and  $\dot{\epsilon}_a^*$  are the strength and conjugate reference strain rate for creep flows, respectively [17].

### 3. AZ31 (Mg-Al-Zn) magnesium alloy

---

### **Experimental procedures**

An AZ31 (Mg-Al-Zn) magnesium alloy used in this study was received in the form of an as-rolled sheet with the thickness of 6 mm. The sheets were first heat treated at 673 K for 100 min to stabilize the microstructure. In order to obtain a fine-grained microstructure capable of undergoing superplastic deformation, a four pass warm rolling was carried out. The thermo-mechanical processing routes shown in table 1 led to a total reduction in thickness from 6 mm to 2.15 mm. The rolled sheets were subsequently heat treated at 523 K for 30 min for stabilization. Plate-type specimens were then machined from the sheets with the dimensions of  $5.0 \times 2.1 \text{ mm}^2$  cross section area with 5 mm and 25 mm gauge length for tensile and load relaxation test, respectively. The loading axis of the specimens was parallel to the rolling direction.

Table 1 Rolling schedule used for grain refinement.

Pass	Reduction rate
1	20%
2	20%
3	20%
4	30%

\* The sheets were heated at 523 K for 30 min before and between each rolling pass and rolls were heated to 373 K

Tensile and load relaxation tests were conducted using a computer controlled electro-mechanical testing machine (Instron 1361 model) equipped with a high temperature furnace capable of maintaining temperature fluctuation within  $\pm 0.5 \text{ K}$ . The tensile tests were conducted at temperatures ranging from 423 to 723 K at strain rates of  $10^{-2} / \text{s}$ ,  $10^{-3} / \text{s}$  and  $10^{-4} / \text{s}$ . A series of load relaxation tests has also been conducted to obtain flow curves in a wider strain rate range with minimal plastic straining, so that the flow behavior can be obtained without changing the internal structure appreciably. High stiffness test machines (INSTRON 8862 & 1361) were used while maintaining the test temperature within  $\pm 0.5^\circ \text{C}$  during the test. Two separate PC were used to control the pre-strain and to record load data as shown in Fig. 3.

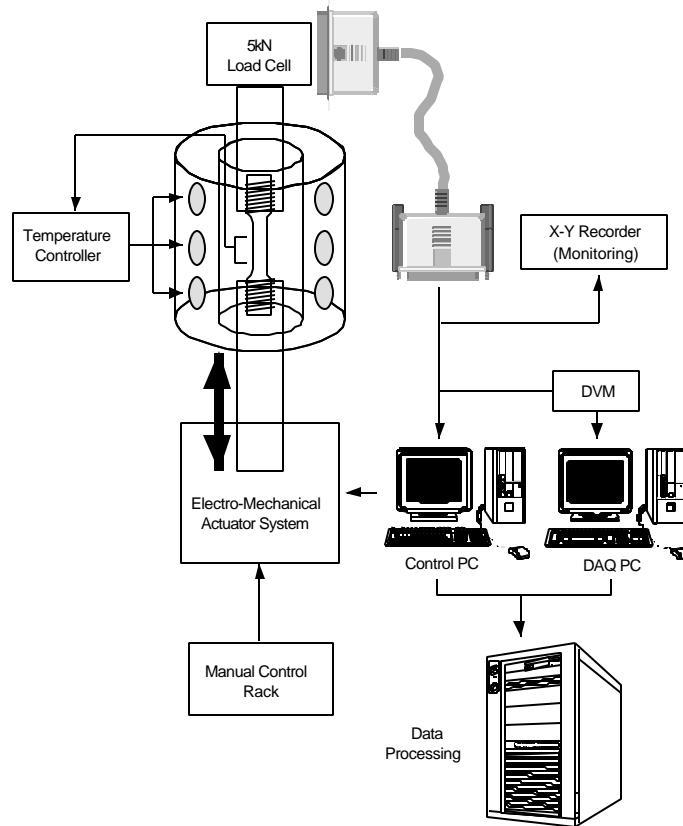


Fig. 3 Schematic diagram of mechanical testing system.

In the load relaxation tests performed in the present study, a specimen was loaded first in tension up to the elongation of 2 % at 423 K, 523 K, 623 K and 723K, followed by stopping the crosshead motion. The variation of load was then recorded in a real time basis at the fixed crosshead position. The flow stress  $\sigma$  and inelastic strain rate  $\dot{\epsilon}$  were then calculated from the load-time data following the usual procedure described by Hart et al. [18]. For determining the effects of strain accumulation, some specimens were preloaded to the elongations of 50 % and 100 % before the load relaxation tests. The furnace temperature of the testing machine was first stabilized for nearly 90 min before starting the high temperature tests. An optical microscope and SEM were then used to observe the microstructures of grip and gauge parts in the tensile and load

---

relaxation specimens after the mechanical tests.

### **Results and discussions**

Microstructures of AZ31 alloy before and after rolling at 523 K are shown in Fig. 4(a) and (b), respectively. The grains before rolling are observed to be coarser and equiaxed in Fig. 4(a), while the resulting microstructure after rolling consists of very fine grains with the average diameter of about 5  $\mu\text{m}$ .

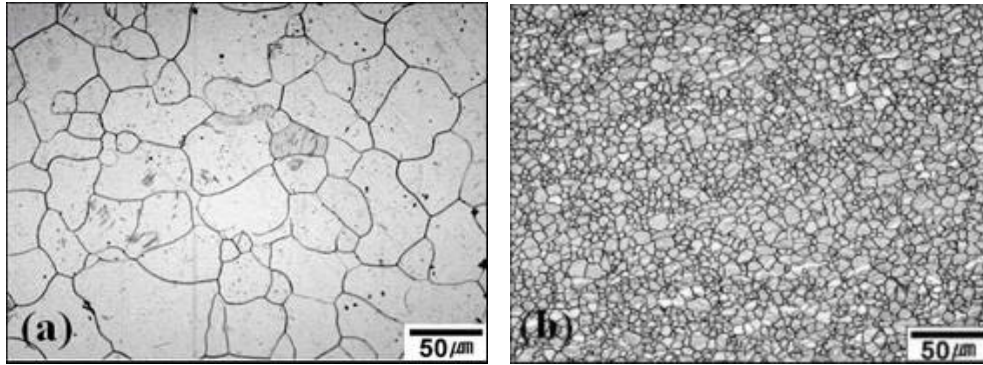


Fig. 4 Microstructures of AZ31 alloy; (a) before and (b) after rolling at 523 K.

The total elongations to failure of the AZ31 alloy are shown in terms of test temperature and strain rate in Fig. 5. The largest tensile elongation of 426 % was obtained at 673 K and  $10^{-4}$  /s. The elongation tends to increase with the increase in test temperature. The test temperature higher than 673 K appears to cause a significant grain growth resulting in the decrease of elongation .

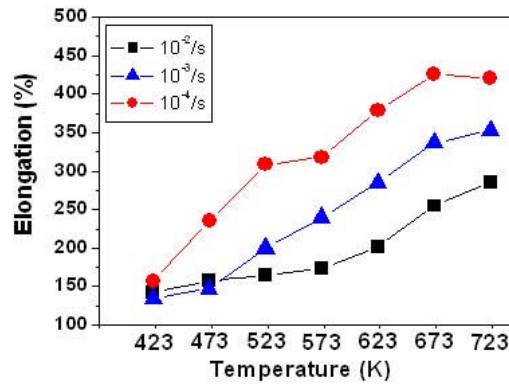
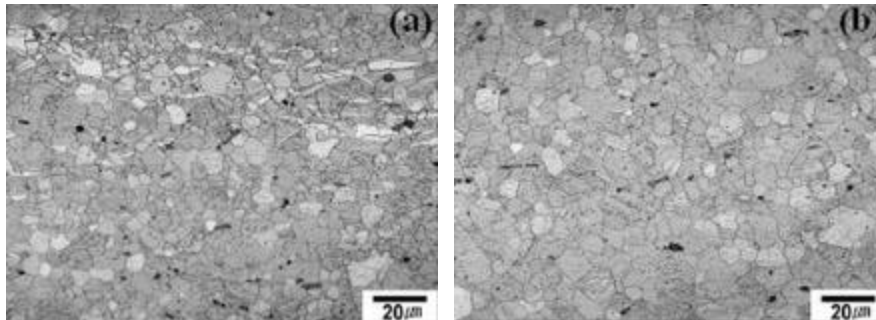


Fig. 5 Total elongation vs. temperature curves at the various strain rates.

Total elongation is observed to become strongly dependent on the strain rate as test temperature is raised, while the deformation behavior is relatively insensitive to strain rate variation at 423 K. The microstructures of grip parts in tensile specimens, tested at the temperatures of 423 K, 523 K, 623 K and 723 K with the strain rate  $10^{-4}$  /s are given in Fig. 6(a)~(d), respectively. The grip parts of these specimens can be regarded as equivalent to static heat treatment with the conditions of 423 K for 320 min, 523 K for 600 min, 623 K for 700 min and 723 K for 750 min. In spite of a much longer heat treating time at 623 K than that at 523 K, grain growth is observed relatively small at 623 K. A few coarser grains are, however, found at 623 K, while a severe grain growth can be observed at 723 K as shown in Fig. 6(d).



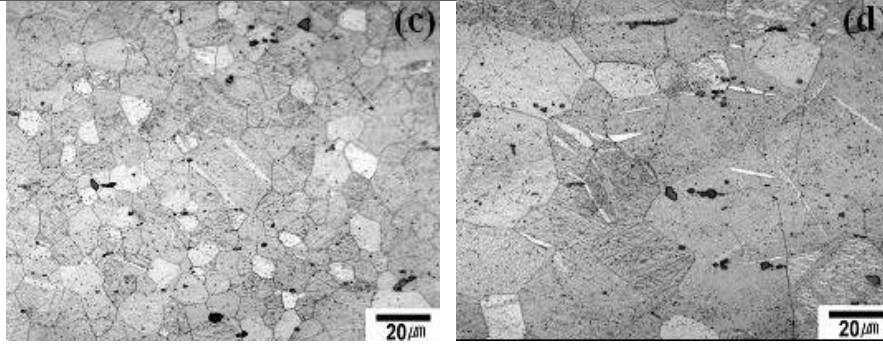
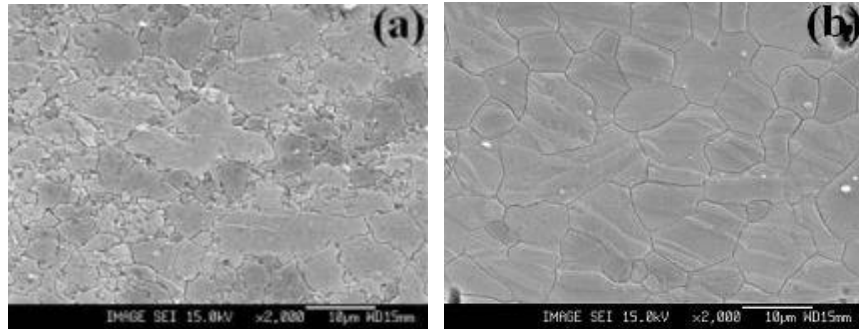


Fig. 6 Grip parts of tensile specimen deformed at (a) 423 K, (b) 523 K, (c) 623 K, and (d) 723 K.

The microstructures of gauge section are given in Fig. 7. The serrated grain boundaries with numerous very fine grains can be clearly recognized in Fig. 7(a), suggesting that DRX process had initiated but not finished yet at 423 K. Smooth grain boundaries are, on the other hand, observed at 523 K as shown in Fig. 7(b) with the microstructure consisting of fine and equiaxed grains, implying dynamic recrystallization (DRX) and GBS as the major deformation mechanisms at 523 K and  $10^{-4}$  /s. Large cavities are observed at the temperatures above 623 K as shown in Fig. 7(c) and (d), possibly caused by GBS [19].



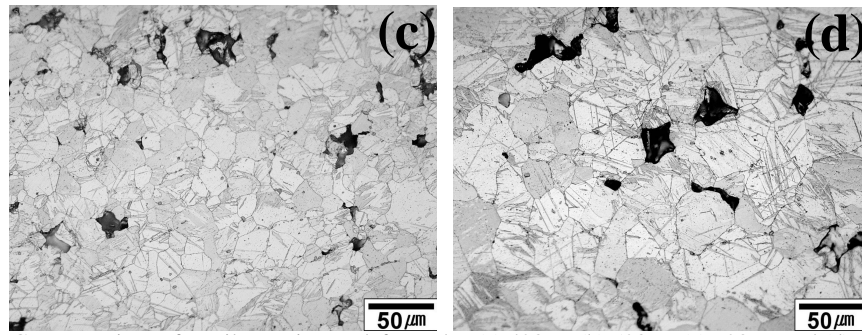


Fig. 7 Gauge sections of tensile specimens deformed at (a) 423 K, (b) 523 K, (c) 623 K, and (d) 723 K.

A load relaxation test can provide flow curves in a much broader range of strain rates with a minimal plastic straining, so that the flow behavior can be obtained without changing the internal structure [12, 14]. Since the grain growth rate of AZ31 magnesium alloys is relatively fast at high temperatures, microstructure investigation must be carried out before and after a load relaxation test to verify the test reliability. The holding time of specimen at the initial temperature was not over 30 min in the relaxation tests. The effect of grain growth during load relaxation test appears to be negligible in the temperature range from 423 K to 623 K by comparing the microstructures before and after load relaxation test. A significant grain growth, however, occurred at 723 K. The flow curves obtained from the relaxation test at the various temperatures and pre-strains are shown in Fig. 8. It is apparent that an increase either in the temperature or strain accumulation tends to shift the flow curves toward the higher stress and higher strain rate region. As described in the previous section, an operation of additional slip systems can be regarded as a main cause for the flow curve shift at higher temperatures. The flow stress at a given strain rate and test temperature is seen to decrease as the amount of pre-strain increases except in the faster strain rate region in Fig. 8. The DRX occurred during the loading period to the pre-strain level is believed to cause the grain refinement [19], consequently shifting flow curves to the higher stress and faster strain rate region.

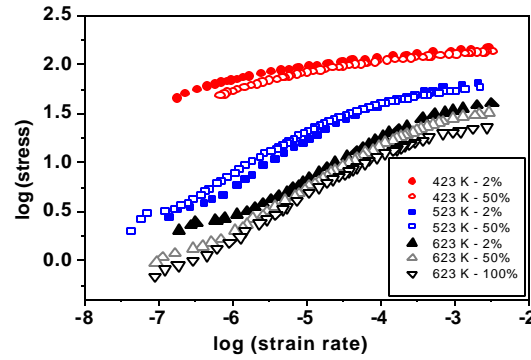


Fig. 8 Flow curves obtained from relaxation tests with the pre-strains of 2 %, 50 % and 100 %.

All flow curves given in Fig. 8 exhibit clearly noticeable concave upward portions within broad strain rate ranges except at 423 K, which is a strong manifestation of GBS in view of the internal variable theory [12]. The flow curves obtained with the 2% pre-strain were analyzed by using the constitutive relations given by Eqs. (3), (5), and (6) and the results are shown in Fig. 9.

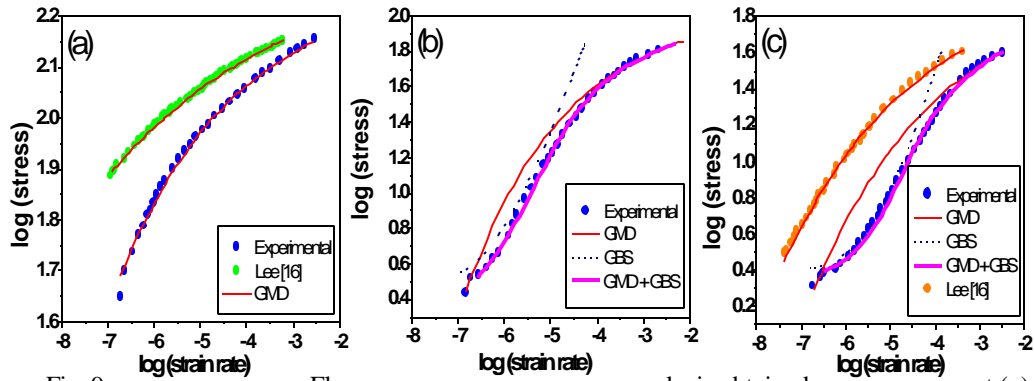


Fig. 9 Flow curve analysis obtained at (a) 423 K, (b) 523 K and (c) 623 K.

The flow curve at 423 K is seen to fit well by the GMD constitutive relation alone given by Eq.

(3), while the curves at 523 K and 623 K are seen to consist of the GMD and GBS contributions. Since the GMD is expected in the regions of higher strain rates and lower stress at 523 K and 623 K, the data in those regions are first used to characterize the deformation process of  $a$  elements. The thin solid lines marked as GMD in Fig. 9 are the predicted curves of  $a$  elements estimated in this way. The strain rate due to GBS ( $g$ ) can then be obtained by subtracting the values of  $a$  from the total inelastic strain rates as prescribed by Eq. (5), assuming  $\dot{\epsilon} \gg 0$ . The GBS curves are then constructed by using Eq. (6) as shown dotted lines in Fig. 9. The constitutive parameters used in Eqs. (3) and (6) can be determined by a nonlinear curve fitting method and the results are listed in Table 2. The bold lines in Fig. 9 represent the composite curves predicted by Eqs. (3), (5), and (6), exhibiting a good agreement with the experimental data. The flow curves at 423 K shown in Fig. 9(a) suggests that GBS does not occur at this temperature, which can easily be verified by the tensile test results and microstructures given in Fig. 5 and Fig. 7(a), respectively.

Table 2 Constitutive parameters determined from the load relaxation tests.

	$\log S^*$	$\log a^*$	$p$	$\log S_g$	$\log g_0$	$M_g$
423 K	2.259	-6.045	0.15			
523 K	2.039	-4.017	0.15	0.441	-6.191	1.0
623 K	2.001	-2.773	0.15	0.378	-5.350	1.0
423 K [20]	2.346	-6.768	0.1			
623 K [20]	2.071	-3.687	0.15			

The upper curve in Fig. 9(a) is the flow curve obtained previously from relaxation test under the same condition for a very coarse-grained AZ91 alloy [20]. By comparing the two flow curves given in Fig. 9(a) and their material parameters listed in table 2, some valuable information such as the effect of grains size on flow behavior can be deduced. The flow curve tends to shift towards to the higher stress and faster strain rate region by reducing the grain size. Another point to be noted here is that the material parameter  $p$  for fine-grained alloy is found to have a different value of  $p = 0.15$  from  $p = 0.1$  obtained for coarse-grained alloy as listed in Table 2. The parameter  $p$  was prescribed to represent dislocation permeability through strong barriers such as grain

boundaries, so that  $p$  value should depend on the properties of boundary and crystal structure. The parameter  $p$  has, on the other hand, been reported to be independent of grain size [13]. The change in  $p$  value is therefore thought to relate with the additional slip systems activated in our fine-grained AZ31 alloy. The coarse-grained AZ91 alloy exhibited much lower elongation of only 62 % at 423 K [20], compared to that of 168 % for fine-grained one used in this study. These results of  $p=0.15$  implies, in turn, indirectly the activation of additional slip systems during the deformation, in contrast to the value of  $p = 0.1$  commonly observed for hexagonal close packed crystals [13, 21], in a good agreement with the previous result [20].

The flow curve analysis obtained at 523 K exhibits a GBS region characterized by a concave upward portion as observed in Fig. 9(b). This in turn implies that this alloy will exhibit superplastic deformation behavior at this temperature, consequently confirmed by the tensile test results and microstructures given in Figs. 3 and 5(b). The GBS region is observed to expand with the temperature increase as can be seen in Fig. 9(c). This result can be related to the deformation behavior at the strain rate of  $10^{-3}$  /s, where the elongation was increased from 134 % to 200 % by increasing the test temperature from 423 K to 523 K (Fig. 3). The extension of GBS region with the increase in temperature implies that the GBS to occur even at the faster strain rate of  $10^{-3}$  /s, resulting into the significantly increased elongation at higher temperatures.

### **Summary**

1. A four pass rolling of AZ31 Mg alloy at 523 K produced fine-grained microstructures and exhibited superplastic deformation behavior with 426 % elongation at 723 K and  $10^{-4}$  /s.
2. The flow stress vs. strain rate curves were found to shift to the higher strain rate and higher stress region by increasing the strain accumulation and reducing grain size as prescribed by the internal variable theory.
3. The permeability parameter  $p$  was found to be 0.15 for a fine-grained AZ31 Mg alloy possibly due to the activation of additional slip systems during deformation.
4. The GBS region is found to enlarge with the temperature increase, resulting in larger elongations at higher strain rates

### **4. Ti-6Al-4V Alloy**

### **Experimental procedures**

A commercial Ti-6Al-4V alloy was first homogenized at 1050 °C for 30 min before cooling with the various cooling rates, viz. water cooling (WC), air cooling (AC), and furnace cooling (FC) to produce different microstructures with various  $\alpha$  phase thicknesses [22, 23]. The alloy was then hot rolled at 700 °C with 60 % reduction before annealing at 800 °C for an hour. After hot rolling, microstructures of the alloys were again observed by an optical microscope and the deformation texture of  $\alpha$  phase developed during hot rolling was measured for (0002) plane by XRD pole figure.

A series of load relaxation tests has been conducted to obtain the flow curves at the various temperatures between 500 °C and 700 °C for specimens with different orientations and cooling rates. Load relaxation test can provide stress-strain rate relations in a much broader range of strain rates with minimal plastic straining [24, 25], enabling to obtain the flow curves without changing the internal structure appreciably [26]. The relaxation data were then consequently analyzed utilizing the internal variable theory for inelastic deformation [10]. Creep tests were also performed to obtain the data in lower strain rate regime and the results were then compared with the relaxation test results.

### **Results and discussions**

The microstructures obtained after furnace cooling (FC), air cooling (AC), water cooling (WC), are shown together with the as-received to exhibit different  $\alpha$  phase thickness in Fig. 10, while the grain size variation after hot rolling is exhibited in Fig. 11. This grain size variation seems to be caused by the different  $\alpha$  phase thickness obtained by changing the cooling rate [22].





Fig. 10 Optical micrographs of (a) As-received, (b) FC, (c) AC and (d) WC specimens.

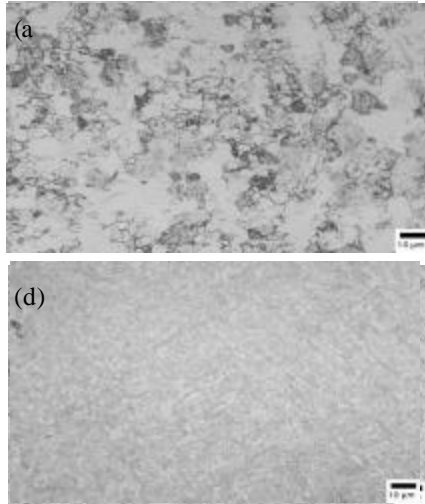
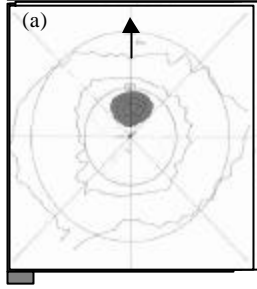


Fig. 11 Microstructures after hot rolling; (a) As-received, (b) FC, (c) AC and (d) WC specimens.

The deformation textures of  $\alpha$  phase after hot rolling are given in Fig. 12. The textures of three heat-treated alloys showed a similar pattern, but non-heat-treated alloy exhibited texture developed only in the normal direction to rolling.



: Intensity > 50 %

Fig. 12 Deformation textures of  $\alpha$  phase after hot rolling; (a) As-received, (b) WC, (c) AC and (d) FC.

The flow curves obtained from load relaxation tests are shown in Fig. 13. The flow stress and the total inelastic strain rate were calculated from the load-time data following the usual procedure described by Lee and Hart [18].

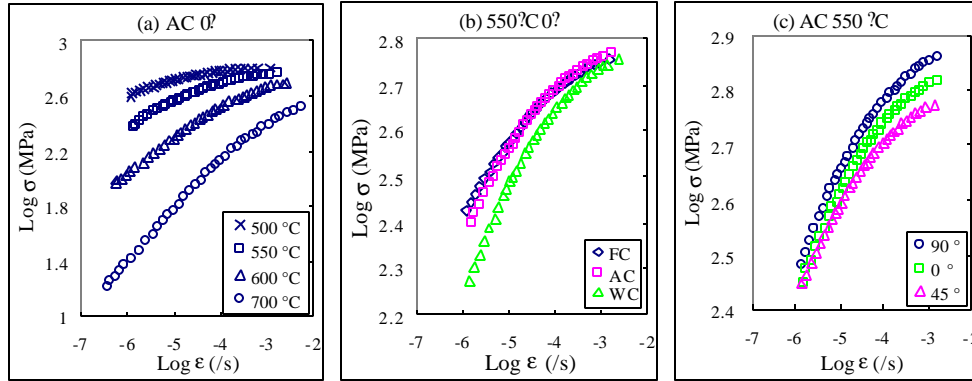


Fig. 13 Variation of flow curves depending on the (a) temperatures, (b) cooling rates and (c) orientations.

The load relaxation test at the high homologous temperature of  $T \geq 0.5T_M$  ensures that the friction stress  $\sigma^F$  is very small compared to  $\sigma^I$  to give  $\sigma \cong \sigma^I$ . Also the tests were performed after the flow stress reached at a nearly steady state to ensure that  $\alpha = 0$  to reduce the Eq. (7) into

$$\dot{\epsilon} = a\sigma + b. \quad (9)$$

These flow curves were then separated into the GMD and dislocation climb contribution by using Eqs. (3) and (8), respectively according to Eq. (9) and a typical analysis result is shown in Fig. 14. The constitutive parameters determined by this analysis are listed in Table 3 through 6.

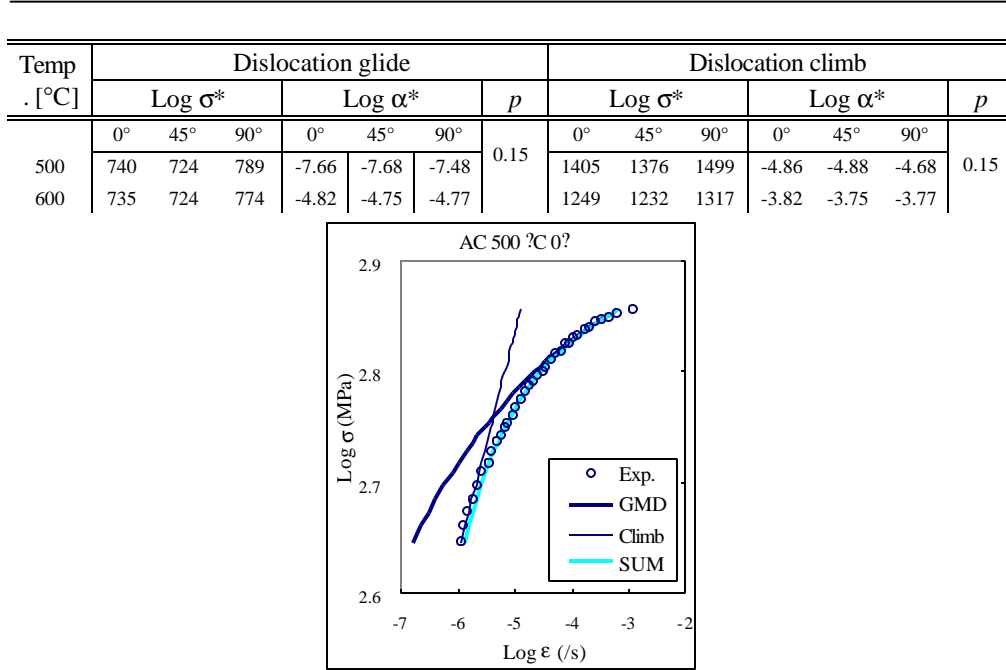


Fig. 14 The flow curve is shown to consist of GMD and dislocation climb contribution.

The value of  $p$  is found as 0.15 as has been reported previously as a characteristic value for cubic crystals [27] and HCP materials [21]. The power exponent  $n$  and  $\alpha^*$  appear not to change significantly with the orientations, but vary with temperatures. The internal strength  $\sigma^*$ , on the other hand, varies with the texture, but not with the temperature.

Table 3 Constitutive parameters of as-received specimen.

Table 4 Constitutive parameters of FC specimen.

Temp : [°C]	Dislocation glide						Dislocation climb							
	Log $\sigma^*$			Log $\alpha^*$			$p$	Log $\sigma^*$			Log $\alpha^*$			$p$
	0°	45°	90°	0°	45°	90°	0.15	0°	45°	90°	0°	45°	90°	0.15
500	745	681	871	-8.46	-8.40	-8.35		1415	1293	1655	-5.66	-5.60	-5.55	
550	743	670	845	-6.70	-6.68	-6.64		1337	1206	1522	-4.70	-4.68	-4.64	
600	736	665	832	-5.37	-5.24	-5.75		1252	1131	1414	-4.37	-4.24	-4.75	

Table 5 Constitutive parameters of AC specimen.

Temp · [°C]	Dislocation glide						Dislocation climb							
	Log $\sigma^*$			Log $\alpha^*$			$p$	Log $\sigma^*$			Log $\alpha^*$			$p$
	0°	45°	90°	0°	45°	90°	0.15	0°	45°	90°	0°	45°	90°	0.15
500	780	695	880	-7.90	-7.82	-7.74		1482	1321	1672	-5.10	-5.02	-4.94	
550	774	692	878	-6.46	-6.70	-6.26		1394	1246	1580	-4.46	-4.70	-4.26	
600	773	690	875	-4.92	-5.30	-4.89		1314	1173	1488	-3.92	-4.30	-3.89	
700	769	685	872	-2.68	-2.96	-2.74		1231	1096	1395	-2.18	-2.46	-2.24	

Table 6 Constitutive parameters of WC specimen.

Temp · [°C]	Dislocation glide						Dislocation climb							
	Log $\sigma^*$			Log $\alpha^*$			$p$	Log $\sigma^*$			Log $\alpha^*$			$p$
	0°	45°	90°	0°	45°	90°	0.15	0°	45°	90°	0°	45°	90°	0.15
500	820	760	925	-6.82	-6.80	-6.89		1559	1445	1757	-4.02	-4.00	-4.09	
550	815	757	910	-5.66	-5.64	-5.92		1466	1362	1638	-3.66	-3.64	-3.92	
600	809	752	906	-4.50	-4.59	-4.47		1375	1278	1540	-3.50	-3.59	-3.47	

The flow stress variations measured at the two different strain rates are plotted in Fig. 15 in terms of temperature to reveal the decreasing tendency of anisotropy with temperature increase due to activation of additional slip systems at higher temperatures [28]. The internal strength  $\sigma^*$  is, however, seen to vary little with temperature from Fig. 16. This in turn implies that the structures of strong barriers acting against the dislocation glide did not change appreciably with temperature in a good agreement with the observation that there was no distinct grain growth or phase fraction change after the tests [21].

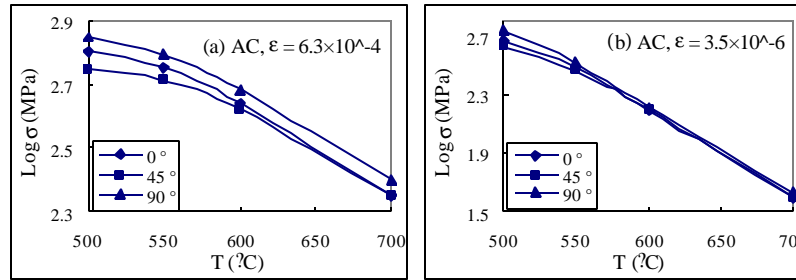


Fig. 15 Variation of flow stress anisotropy measured at (a)  $\epsilon = 6.3 \times 10^{-4}$  and (b)  $\epsilon = 3.5 \times 10^{-6}$ .

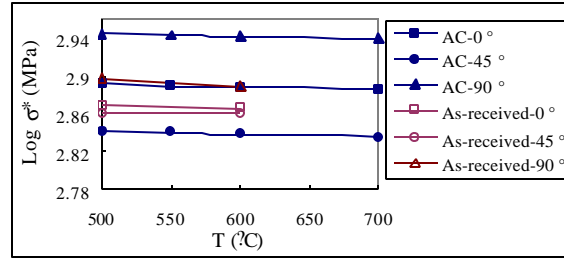


Fig. 16 Internal strength parameter  $\sigma^*$  is plotted as a function of test temperature.

The power law exponents  $n$  can be observed to vary from 5-6 at 500 °C to 3-4 at 600 °C to suggest that the dislocation climb is more activated. And a rather large dependence to test orientation at low temperatures, as shown in Fig. 15, implies that dislocation glide is main deformation mechanism, while the disappearance of orientation dependence at higher temperatures provides an indirect evidence for dislocation climb as diffusion process. A significant orientation dependence of internal strength  $\sigma^*$  can also be observed from Fig. 16 for both the as-received and AC specimens, but the as-received specimen has less orientation dependence than the others as expected from the features of texture formed given in Fig. 12.

The results of creep tests, performed to obtain data of low strain rate regime, are shown in Fig. 17. The time to reach to 1 % plastic creep strain seems to depend on the test directions, again suggesting main deformation mode by dislocation glide. Creep test results in Fig. 17(b) show that the effect of texture is reduced by lowering stress and raising temperature and it is explained from the former load relaxation test that dislocation climb is more activated. These results are in agreement with the result of load relaxation tests.

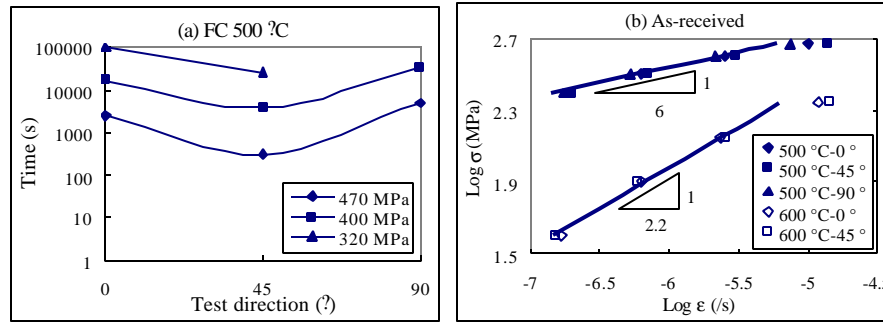


Fig. 17 Creep test results; (a) Times to reach 1 % plastic creep strain and (b) the power law exponents at 500 °C and 600 °C.

### Summary

1. Microstructures with different  $\alpha$  phase thickness were obtained by varying the cooling rate, which in turn produced various textures after hot rolling.
2. Flow curves obtained from load relaxation tests revealed quantitatively their dependence on microstructures, test temperatures, and textures.
3. The internal strength variable  $\sigma^*$  was found to vary significantly by the textures, but not by test temperature, while the texture effect was found to decrease at higher temperatures.
4. The effect of texture was also observed to decrease by raising test temperature or by reducing the applied stress in creep tests, suggesting that glide assisted dislocation climb was activated at higher temperature and lower stress.

### 5. References

1. Y. N. Wang and J. C. Huang; Metall. Mater. Trans., 35A (2004) 555.
2. Manping Liu et al.; Metals and Materials Int., 6 (2002) 2433.
3. Sugui Tian et. al.; Mater. Sci. Eng., 415A (2005) 309.
4. H. Watanabe, T. Mukai, M. Mabuchi, and K. Higashi; Acta Mater., 49 (2001) 2027.
5. H. Watanabe, T. Mukai, M. Koichi Ishikawa, and K. Higashi; Scripta Mater., 46 (2002) 851.
6. H. Watanabe, H. Tsutsui, T. Mukai, M. Kohzu, S. Tanabe, and K. Higashi; Int. J. plasticity, 17 (2001) 387.
7. H. Watanabe, T. Mukai, M. Kohzu, S. Tanabe, and K. Higashi; Acta Mater., 47 (1999) 3753.

- 
8. Y. N. Wang and J. C. Huang; Metall. Mater. Trans., 35A (2004) 555.
  9. W. J. Kim, S. W. Chung, C. G. Chung, and D. Kum; Acta Mater. 49 (2001) 3337.
  10. T. K. Ha and Y. W. Chang; Acta Metall., 46 (1998) 2741.
  11. J. H. Kim, S. L. Semiatin, and C.S. Lee; Acta Mater., 51 (2003) 5613.
  12. T. K. Ha, H. J. Sung, K. S. Kim, and Y. W. Chang; Mater. Sci. Eng. 271A (1999) 160.
  13. T. K. Ha and Y. W. Chang; Scripta Mater., 41 (1999) 103.
  14. T. K. Ha, H. W. Koo, and Y. W. Chang; Metals and Materials Int., 9 (2003) 29.
  15. J. S. Park, W. Bang, and Y. W. Chang; Key Eng. Mater., 274 (2004) 301.
  16. E.W. Hart; J. Eng. Mater. Tech., 106 (1984) 322.
  17. J. H. Song, T. K. Ha, and Y. W. Chang; Scripta Mater., 42 (2000) 271.
  18. D. Lee and E.W. Hart; Metall. Trans., 2A (1971) 1245.
  19. J. C. Tan and M. J. Tan; Mater. Sci. Eng., 339A (2003) 81.
  20. H. S. Lee, W. Bang, and Y. W. Chang; Trans. Mater. Processing, 13 (2004) 535.
  21. J. H. Kim, S. L. Semiatin, and C.S. Lee; Acta Mater., 51 (2003) 5613.
  22. S. L. Semiatin and T. R. Bieler; Acta Mater., 49 (2001) 3565.
  23. K. S. Park and S. K. Lee; Metals Mater. Int., 11 (2005) 481.
  24. E. W. Hart; *Stress relaxation testing*, ed. A. Fox, ASTM Special Tech., 676 (1979) 5.
  25. R. Enrique and P. P. Gillis; Metall. Trans., 22A (1991) 2302.
  26. S. H. Chon and J. K. Park; Metals Mater. Int., 10 (2004) 567.
  27. Y. N. Kwon and Y. W. Chang; Metall. Trans., 30A (1999) 2037.
  28. J. S. Lecomte; Mater. Sci. Eng., 234-236 (1997) 869.

## 6. Publications and presentations

### 1. AZ31 Mg alloy

- TMS 2005 Annual Spring Meeting in San Francisco, CA
- “Creep Transition Behavior of Magnesium Poly and Single Crystals ”
- J. S. Park and Y. W. Chang

– **THERMEC 2006** in Vancouver, Canada, July 4-7

“Constitutive Analysis for Superplastic Deformation Behavior of AZ31 Magnesium Alloy”

H. S. Lee, W. Bang, D. W. Kim S.L. Semiatin, and Y. W. Chang

– **AFDM 2006** in Busan, Korea, September 4-6

**Plenary lecture:** “High Temperature Deformation Behavior of Mg alloys”

## **2. Ti-6Al-4V alloy**

– **AEPA 2006** in Nagoya, Japan, September 25-29

1) **Plenary lecture:** “An Internal Variable Approach to Inelastic Deformation including Structural Superplasticity”

2) “Effect of Texture on High Temperature Mechanical Properties of Ti Alloys”  
J. E. Park and Y. W. Chang